Chemical Engineering Science 193 (2019) 53–65

Contents lists available at ScienceDirect

Chemical Engineering Science

journal homepage: www.elsevier.com/locate/ces

Study of hydrodynamics in wave bioreactors by computational fluid dynamics reveals a resonance phenomenon

Caijuan Zhan [a,b,c,d], Erika Hagrot [a,b], Luca Brandt [d], Veronique Chotteau [a,b,c,*]

[a] Cell Technology Group (CETEG), Dept. of Industrial Biotechnology, School of Engineering Sciences in Chemistry, Biotechnology and Health, KTH-Royal Institute of Technology, SE-10691 Stockholm, Sweden
[b] AdBIOPRO, VINNOVA Competence Centre for Advanced Bioproduction by Continuous Processing, Sweden
[c] Wallenberg Centre for Protein Research (WCPR), SE-10691 Stockholm, Sweden
[d] Linné FLOW Centre, KTH Mechanics, Royal Institute of Technology, SE 10044 Stockholm, Sweden

HIGHLIGHTS

- A resonance phenomenon can occur in Wave bioreactor.
- This resonance phenomenon can create higher shear stress for lower agitation speed.
- The fluid hydrodynamics is characterized for 9 operating conditions by CFD.
- The studied shear stress range can be detrimental for adherent cell cultures.

GRAPHICAL ABSTRACT

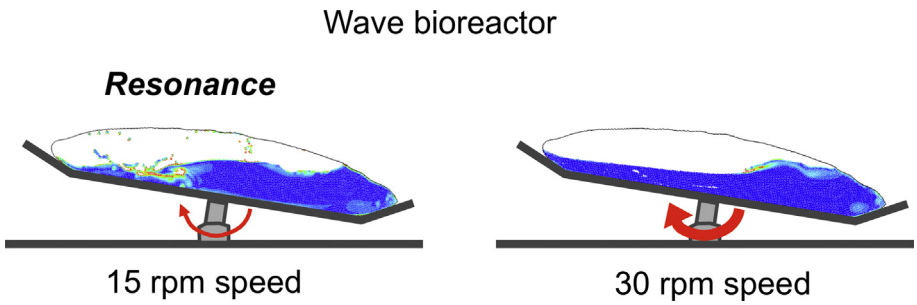

ARTICLE INFO

Article history:
Received 15 March 2018
Received in revised form 2 August 2018
Accepted 7 August 2018
Available online 10 August 2018

Keywords:
Wave bioreactor
Computation Fluid Dynamics (CFD)
Volume of fluid (VOF)
Hydrodynamic
Resonance

ABSTRACT

Culture of mammalian or human cells in Wave bioreactor is widely used for cell expansion or for biologics manufacturing. Wave bioreactor cultivation of sensitive cells such as stem cells, immune cells or anchorage-dependent cells, is recognized as an attractive option for culture in suspension or adherently on microcarriers. A systematic optimization of the mixing, oxygen transfer rate and shear stress, most favorable for the cells requires a deep understanding of the hydrodynamics inside the Wave bioreactor bag, i.e. cellbag. Numerical simulation by Computation Fluid Dynamics (CFD), is considered as an inexpensive and efficient tool for predicting the fluid behavior in many fields. In the present study, we perform numerical simulations by Ansys-FLUENT to characterize the flow conditions in a 10 L cellbag. The numerical simulations are carried out to investigate the fluid structures for nine different operating conditions of rocking speed and angle. The influence of these operating parameters on the mixing and the shear stress induced by the liquid motion are studied. We find that the mixing and shear stress increase with the cellbag angle from 4° to 7° but that increasing rocking speeds are not systematically associated with increasing mixing and shear stress. It is concluded that a resonance phenomenon is responsible for the fact that the lowest studied rocking speed, 15 rpm, generates the highest fluid velocity, mixing and shear stress compared to the higher speeds of 22 and 30 rpm.

1. Introduction

The interest in single-use equipment has tremendously increased since the introduction of the disposable bioreactors. This technology reduces the procedures of cleaning and sterilization, the cross-contamination validation, the risk of contamination, and

Abbreviations: CFD, Computational Fluid Dynamics; PRESTO!, Pressure Staggering Option; UDF, user-defined functions; VOF, volume of fluid.

* Corresponding author at: Cell Technology Group (CETEG), Dept. of Industrial Biotechnology, School of Engineering Sciences in Chemistry, Biotechnology and Health, KTH-Royal Institute of Technology, SE-10691 Stockholm, Sweden.
E-mail address: chotteau@kth.se (V. Chotteau).

https://doi.org/10.1016/j.ces.2018.08.017
0009-2509/

Nomenclature

A	rocking angle, °
A_{area}	surface area, m^2
C^*	saturated dissolved oxygen concentration in liquid phase
C_L	oxygen concentration
$\vec{f}$	body force exerted on fluid, N
g	gravity, m/s^2
H	height between two outer plates to measure the cellbag, m
H_1	distance between the upper cellbag surface and the upper plate, m
H_2	distance between the lower cellbag surface and the lower plate, m
h	height of liquid phase in the tank, m
K_La	oxygen transfer rate coefficient, h^{-1}
L	characteristic length of the bag, m
P	pressure, Pa
Re	Reynolds number
S	rocking speed, rpm
t	time, s
T	cycle time of rocking motion, s
$\vec{\mathbf{u}}$	fluid velocity vector
u_x	fluid velocity in x direction, m/s
u_y	fluid velocity in y direction, m/s
u_z	fluid velocity in z direction, m/s
Wo	Womersley number

Greek letters

α	volume fraction
β	arbitrary parameter
Δx	the maximum fluid element displacement in the vessel during one cycle, m
μ	liquid dynamic viscosity, Pa s
ν	kinematic viscosity, m^2/s
$\boldsymbol{\omega}$	vorticity, s^{-1}
ρ	density, kg/m^3
τ_{ij}	shear stress tensor, Pa s
$\dot{\theta}$	angular speed of the rocking motion, rad/s

enhances the process safety (Eibl et al., 2009). It has been estimated that the cost savings are larger than 60% with single-use systems compared to stainless-steel based equipment in biopharmaceutical manufacturing (Morrow, 2006). An ideal bioreactor should be perfectly mixed however with shear stress not damageable for the cells.

In 1999, Singh (1999) introduced the disposable wave-induced bioreactor, consisting of a bag on a rocking tray agitating the cell culture with a back and forward wave-like movement. The Wave bioreactor, designed to provide excellent mixing and gas transfer with reduced shear stress, can provide an interesting alternative for the culture of cells highly sensitive to hydrodynamic conditions. The design of this bioreactor is simpler than the stirred bioreactor due to the absence of a sparger and, presently, these systems are available up to working volumes of 500 L.

Various examples demonstrating the possibility to adapt processes performed in stirred tank bioreactors or roller bottles to the Wave bioreactor have been reported for the culture of animal cells (Hundt et al., 2007, Okonkowski et al., 2007, Lohr et al., 2009, Clincke et al., 2013a,b). The Wave bioreactor is often used for the production of immune cells, stem cells or viral vectors for cell therapy, gene therapy or vaccine, since it is disposable and it generates satisfying culture homogenization, potentially at low shear stress (dos Santos et al., 2013, Liu et al., 2014, Schnitzler et al., 2016). Among these, cells adhering on a support such as microcarriers are much more sensitive to shear stress than suspension cells, as reviewed by Chalmers (2015). Ma et al. (2002) experimentally demonstrated that CHO cells, i.e. single cells, in suspension are four to five orders of magnitude less sensitive to energy dissipation rate (as measure of extensional and shear stress) than CHO cells adhering on microcarriers of 200 μm diameter. Wave bioreactors have been shown to be very adequate for the cultivation of cells on microcarriers (Chen et al., 2013, Liu et al., 2014, Genzel et al., 2006).

Computational Fluid Dynamics (CFD), also known as 'numerical experiments', is considered to be an inexpensive and effective way to analyze and visualize the impact of hydrodynamic forces and shear stress (Sharma et al., 2011). Its potential for flow optimization without performance of expensive experimental studies increasingly attracts scientists. CFD modeling can overcome experimental limitations and enables a full characterization of three-dimensional flow fields in bioreactors with simple and complex geometries. Williams et al. (2002) applied Fluent CFD models to calculate flow fields, shear stress, and oxygen profiles around non-porous constructs, which simulated the cartilage development in a concentric cylinder bioreactor. Their mass transport modeling for oxygen demonstrated that the fluid-phase oxygen transport to the constructs was rather uniform, leading to the conclusion that, in this bioreactor, chondrocyte growth would not be subject to oxygen limitation. Other examples can be found for instance in the review of Singh and Hutmacher (2008).

Numerical simulations of the Wave bioreactor (e.g. cellbag) hydrodynamics have confirmed CFD as a reliable method (Öncül et al., 2010). This group numerically investigated the key flow properties in the Wave bioreactors for two reactor sizes (2 L and 20 L cellbags) at the agitation of 15 rpm and 7° motion angle, using the CFD code ANSYS-FLUENT 6.3. Their results showed that the flows stayed in the laminar regime, confirming that gentle mixing conditions took place. These authors also found that the shear stress levels were below known threshold values leading to damage of animal cells.

The purpose of the present study is to provide a better understanding of the effect of the agitation and the rocking angle on the key flow properties in the Wave bioreactor using CFD. CFD numerical simulations are performed using Ansys-FLUENT 13.0 in a 10 L cellbag of a Wave bioreactor to study the fluid velocity, mixing, shear stress and vorticity in different operating conditions. The distribution and intensity of the high stress regions are numerically computed for different agitation conditions. Finally, the oxygen transfer coefficient, K_La, is measured and compared to a simulation of the amount of gas held in the liquid phase, i.e. gas hold-up.

2. Numerical methodology and measurement of oxygen transfer rate

In this section, the numerical methods and models used for the simulation of the fluid flow in a Wave bioreactor cellbag are presented.

2.1. Simulation domain and mesh

The first step, essential for the precision of the numerical simulation, is to establish the geometry of the simulation domain.

We manually measure the geometry of an inflated cellbag (10 L cellbag of a Wave bioreactor 20/50, GE Healthcare). This bag is considered as rigid body in the simulations (Öncül et al., 2010). The bag is made with a rather stiff plastic sheet and in operation it is constantly under overpressure by a continuous gas inlet and reducing outlet gas valve. Consequently, for a small volume bag such as used in the present study, the geometry does not noticeably change and considering the bag as a rigid body has a negligible effect on our simulation results for this bag volume. The method to measure the geometry is illustrated in Fig. 1.

A 10 L cellbag filled with 5 L water is placed on the bottom plate (Plate 1), where a uniformly distributed grid is drawn. A second similar board (Plate 2) is placed above the bag at a given height H (0.5 m). For all the nodes of the grid, the vertical distance between the upper plate and the bag upper surface (i.e. upper height H_1), as well as the vertical distance between the lower plate and the bag lower surface (i.e. lower height H_2), are measured by calipers and recorded. The measurements are performed in triplicates of which an average value is taken. Once the measurements of all the nodes are done, the simulation domain of the cellbag is generated by ICEM-CFD. By defining the lower surface as a XZ plane, the lower and upper surface of the cellbag are generated with the values of $y_1 = H_2$ and $y_2 = H–H_1$, respectively. The geometry is in the simulation domain of $(-0.23,\ 0.23) \times (0,\ 0.0854) \times (-0.15,\ 0.15)$ m. To achieve a good numerical resolution, a fine unstructured mesh of 1 707 248 cells shown in Fig. 2, is generated.

2.2. Governing equations

The time-dependent, three-dimensional Navier-Stokes equations together with relevant boundary conditions contain all the physics of a given fluid flow. It is assumed that the cellbag system consists of two incompressible and immiscible fluids, the liquid phase and the gas phase. The transport of momentum for the incompressible, isothermal flow of Newtonian fluids can be described as:

$$\nabla \vec{\mathbf{u}} = 0 \tag{1}$$

$$\frac{\partial \vec{\mathbf{u}}}{\partial t} + \vec{\mathbf{u}} \nabla \vec{\mathbf{u}} = -\frac{\nabla P}{\rho} + \nu \nabla^2 \vec{\mathbf{u}} + \vec{f} \tag{2}$$

where $\vec{\mathbf{u}}$ is the fluid velocity vector, ν is the kinematic viscosity, P is the pressure, ρ is the density and t is time. $\vec{f}$ is an additional body force, the gravity in the present case. During the wave motion of the bag, the gravity force g is decomposed into x and y direction.

$$\text{x } direction: \quad -g \sin\theta = -g \sin(\dot{\theta} t) \tag{3}$$

$$\text{y } direction: \quad -g \cos\theta = -g \cos(\dot{\theta} t) \tag{4}$$

where $\dot{\theta}$ is the angular speed of the rocking motion, calculated from the rocking speed and angle as follows:

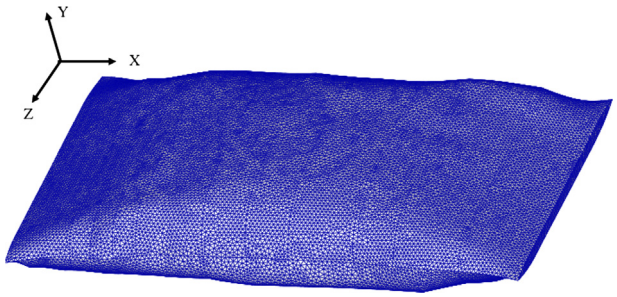

Fig. 2. Unstructured mesh of 1 707 248 cells used for the numerical simulation of the cellbag.

$$\dot{\theta} = \frac{4A2\pi}{360T} = \frac{AS\pi}{2700} \tag{5}$$

with the rocking angle A and the oscillation period T = 60/S, where S is the rocking speed expressed in revolution per minute (rpm).

The volume of fluid (VOF) method, which relies on the fact that two or more fluids (or phases) are not interpenetrating, is widely used as a free-surface modeling technique since several decades (Noh and Woodward, 1976). For each additional phase added to the model, a new variable is introduced: the volume fraction of the phase in the computational cell. In each control volume, the volume fractions of all the phases sum to unity. The fields for all the variables and properties are shared by the phases and represent volume-averaged values as long as the volume fraction of each phase is known at each location. Thus, the variables and properties in any given cell are either purely representative of one of the phases, or representative of a mixture of the phases, depending upon the volume fraction values. Mathematically, this model can be written as follows:

$$\sum_{k=1}^{n} \alpha_k = 1 \tag{6}$$

$$\frac{\partial \alpha_k}{\partial t} + u \nabla \alpha_k = 0 \tag{7}$$

$$\rho = \alpha_2 \rho_2 + (1 - \alpha_2) \rho_1 \tag{8}$$

where α_k is the volume fraction of the k_{th} phase ($k = 1, 2$). In the VOF model, a single momentum equation is solved throughout the domain and the resulting velocity field is shared among the phases. This method is adopted in the present simulations to track the interface between liquid and gas, i.e. between two phases, during the wave motion in the cellbag.

2.3. Numerical methods

All the simulations are performed using the CFD code ANSYS-FLUENT 13.0. In order to describe the free liquid surface in an unsteady manner, the three-dimensional calculations employ the

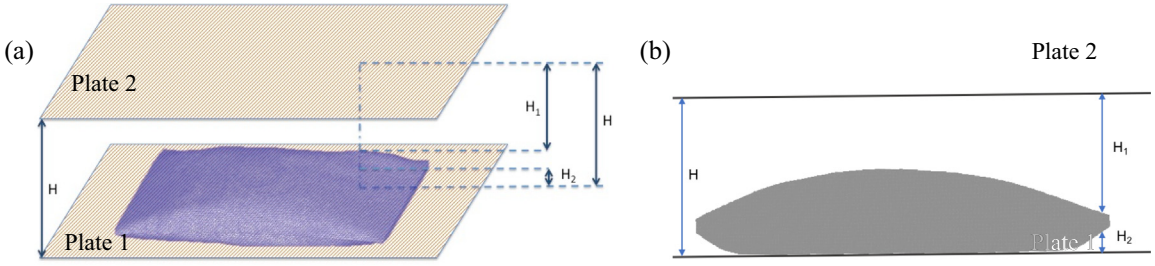

Fig. 1. Illustration of the method used to measure the geometry of the cellbag.

VOF method, leading to higher computational costs. The VOF method enables to solve the governing equations on a fixed mesh, without the need of conforming to the interface deformation. In this approach, the liquid surface is identified by the value of the local volume fraction.

The PRESTO! (Pressure Staggering Option) scheme is used for the pressure-velocity coupling. The PRESTO! discretization calculates the pressure on the liquid surface using a staggered grid where the velocity and pressure variables are not "co-located". Notice that the PRESTO! discretization gives very accurate results since the interpolation errors and pressure gradient assumptions on boundaries are avoided. The solver is implicit and segregated with a time integration being first order implicit.

In order to specify the state of the flow inside the cellbag, we need a non-dimensional number to quantify the onset of turbulence. During the operations, the Wave bioreactor has a one-dimensional rocking motion. Kurzweg et al. (1989) proposed to estimate the turbulence onset in unsteady oscillating flow as a function of the Womersley number (*Wo*) and of the parameter β, defined as follows

$$Wo = \frac{L}{2}\sqrt{\frac{\dot{\theta}}{\nu}} \tag{9}$$

$$\beta = \Delta x\sqrt{\frac{\dot{\theta}}{\nu}} \tag{10}$$

where L denotes the characteristic length scale of the flow (which is, in our case, given by length of the cellbag), Δx indicates the maximum fluid element displacement in the vessel during one cycle, and $\dot{\theta}$ is the angular speed of the oscillations calculated in Eq. (5).

The operating conditions considered in the present work assume angles between 4° and 7° and speeds between 15 rpm (rpm) and 30 rpm, based on the most common operating conditions used in the field with this equipment and corresponding as well to the supplier recommendation. In this range, the angular speed, $\dot{\theta}$, lies between 0.0698 and 0.2443. The cellbag is filled with 5 L liquid, resulting in Δx of 0.038 m. In these conditions, the maximum value of *Wo* is 9.39. A value $Wo > 1$ corresponds to a flow strongly modified by unsteady effects, which is the case in the present configuration. In the definition of the parameter β (Eq. (10)), Δx indicates the maximum fluid element displacement in the vessel during one cycle and is taken as the length of the cellbag, leading to a maximal value of β of 22.74. Turbulence first appears in oscillating flows when β exceeds 700 for $Wo \geq 8.5$ (Kurzweg et al., 1989). Thus, with the selected settings, the present system

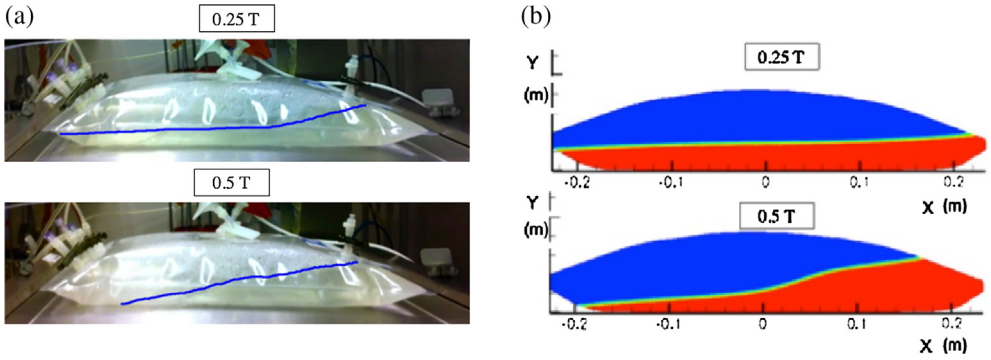

Fig. 3. Phase distribution in a Wave bioreactor cellbag with a speed of 30 rpm and angle of 7° in 5 L volume captured by filming an experiment (a) and by 3D simulations (b) at time 0.25 T (top figures) and time 0.5 T (lower figures).

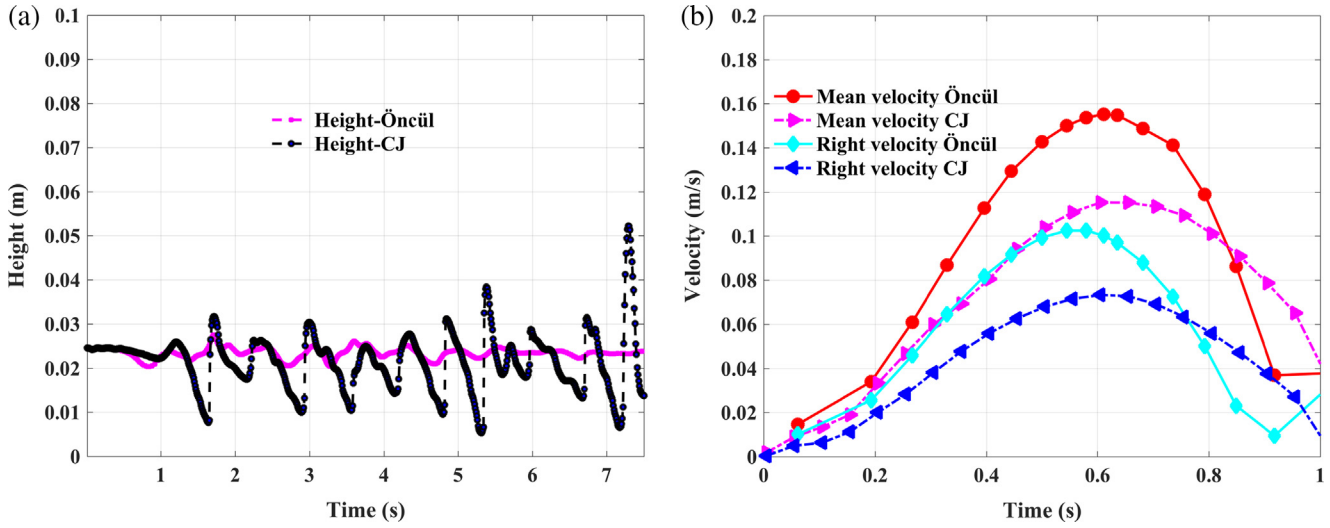

Fig. 4. 3D simulation results of (a) interface height and (b) liquid velocity spatial distribution in 2 L cellbag using the simulation geometry from Öncül (Öncül et al., 2010) for speed 30 rpm and angle 7° and the geometry generated in the present study, denoted 'CJ'.

cannot be considered as turbulent and the simulations do not include any turbulence model.

The rocking motions in the different conditions are defined by user-defined functions (UDF), given by Eqs. (3) and (4).

2.4. Measurement of oxygen transfer rate

The oxygen transfer rate coefficient K_La is measured in pure water. The oxygen concentration is monitored in the liquid phase by a dissolved oxygen probe calibrated at 100% air. The rate of oxygen transfer from the gas phase to the liquid phase can be described by the equation

$$\frac{dC_L}{dt} = K_La(C^* - C_L) \tag{11}$$

where C_L is the oxygen concentration and C^* is the air-saturated dissolved oxygen concentration in the liquid phase. In the experiments, a constant air flow is maintained at all times.

3. Results and discussions

3.1. Validation of the model

The numerical models and simulations are qualitatively and quantitatively validated by comparing the simulations of the liquid motion in the Wave bioreactor cellbag with phase capture images taken during the experiments on one hand and with the results using the geometry from the study of Öncül et al. (2010) on the other hand. For the latter, our simulations are performed using the simulation domain in the geometry of Öncül et al. and for the same operating conditions.

Fig. 3 shows a qualitative comparison of the air-water interface from experimental images and simulation results taken at the same time point, with the same conditions of speed 30 rpm and angle 7°. A good agreement of the air-water interface between the simulation and the images is observed.

For a quantitative validation purpose, the simulation results generated by our geometry and numerical model are compared to the results of Öncül using the geometry of their study (Öncül et al., 2010), which has been kindly provided by Prof. D. Thevenin's group. Fig. 4(a) shows a comparison of the water-air interface height. It can be seen that the trend is similar, however, there are larger oscillations in our model. This could be due to the smaller mesh size used in our simulations, leading to a higher numerical resolution. Fig. 4(b) presents the average velocity in the liquid phase and shows that the general trends of the velocity as function of time are similar. The difference between the two numerical models, the one developed here and the one presented by Öncül, is 20% on average. Since smaller time steps are used in the present simulation compared to the model of Öncül, smoother variations are observed in our results.

The complex geometry and the large amount of nodes make the 3D simulations highly time consuming and not practically feasible for a large number of operating conditions. For this reason, taking advantage of the symmetric shape of the cellbag, it is evaluated if the present study can be performed with 2D (two dimensional) simulations instead of 3D. The 2D simulation domain is taken as the cross section of the cellbag along a vertical plane at the middle of the bag breadth with outer dimensions $(-0.23, 0.23) \times (0, 0.0854)$ m. The 2D simulation is compared to 3D simulation for a speed of 30 rpm and angle of 7°. The evolution of the velocity of two points, p1 and p2, working as virtual probes in the cellbag is represented for 3D- and 2D simulations from the second cycle time in Fig. 5. The points p1 and p2 are taken in the liquid phase at (0, 0.01, 0) and (0.05, 0.02, 0) defined at time zero. The velocities obtained by 2D- and 3D simulations have similar trends and are in phase. The average difference between both simulations is 20%, which can be attributed to the complex geometry of the cellbag. It is deemed that the 2D simulation can be used as a valid tool to simulate the trends of the liquid hydrodynamics in the cellbag. Following this, 2D simulations are performed as listed in Table 1 at working volume of 5 L with nine combinations of three values of speed (15, 22 and 30 rpm) and three values of rocking angle (4°, 5.5° and 7°).

3.2. Mixing and shear stress

The mixing and the shear stress are important parameters to obtain a satisfying culture homogenization but can potentially generate cell damage. In this section, these parameters are studied for different operating conditions and their behavior is analyzed using the simulation data.

3.2.1. Mixing

In a bioreactor, the mixing is a physical process aiming at reducing the non-uniformities in the fluid by eliminating the gradients of substrates, by-products, temperature, pH, dissolved oxygen concentration, etc. To a very large extent, the mixing determines the

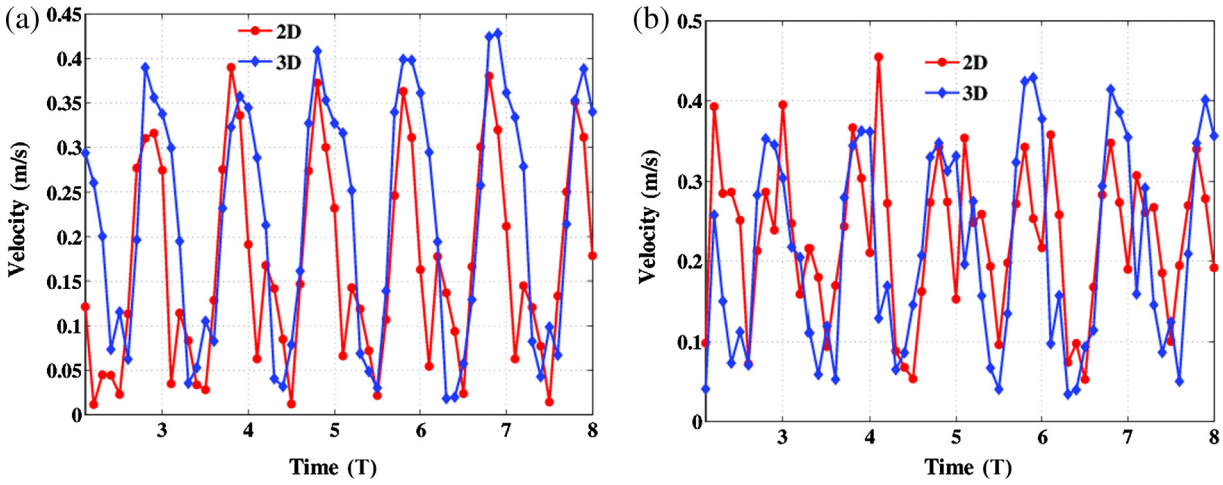

Fig. 5. Velocity of the points (a) p_1 (0, 0.01, 0) and (b) p_2 (0.05, 0.02, 0) defined at time zero, at speed 30 rpm and angle 7° in 5 L volume by 3D and 2D simulations represented as a function of time from the second cycle 2 T.

Table 1
Operating conditions for 2D simulations.

Speed (rpm)	Angle (°)	Volume of fluid
15	4, 5.5, 7	5 L
22	4, 5.5, 7	5 L
30	4, 5.5, 7	5 L

performance of a bioreactor. It can be described as a combination of three physical important factors: the distribution, the dispersion and the diffusion. The process whereby materials are transported to all the regions of the vessel by bulk circulation currents is the distribution, which is generated by the fluid circulation. In the cellbag, the rocking motion generates a rocking force responsible for the fluid circulation. The velocity distribution is very important for the bioreactor mixing.

Fig. 6 shows 2D simulation of the velocity distribution forced by the rocking motion of the cellbag during the 4th cycle, at speed 30 rpm and angle 7°. The region of high velocity lies along the gas–liquid interface and is more likely located in the gas phase. This is due to the conservation of the momentum along this interface. Since gas has a lower density compared to liquid, it has a higher velocity.

To further characterize the fluid properties, the Reynolds number, *Re*, is computed based on 2D simulation. As illustrated in Fig. 7, *Re* is mostly determined by the speed and varied between 3000 and 20,000 during the 5th cycle. It is most of the time highest for 15 rpm speed while it is in a lower and similar range for the speeds 22 and 30 rpm (Fig. 7a). *Re* increases with the angle as exemplified in Fig. 7b. According to the analysis in Section 2.3, the liquid flow in the present system is not turbulent but laminar. In light of this, the observed large Reynolds numbers, in particular at 15 rpm, imply

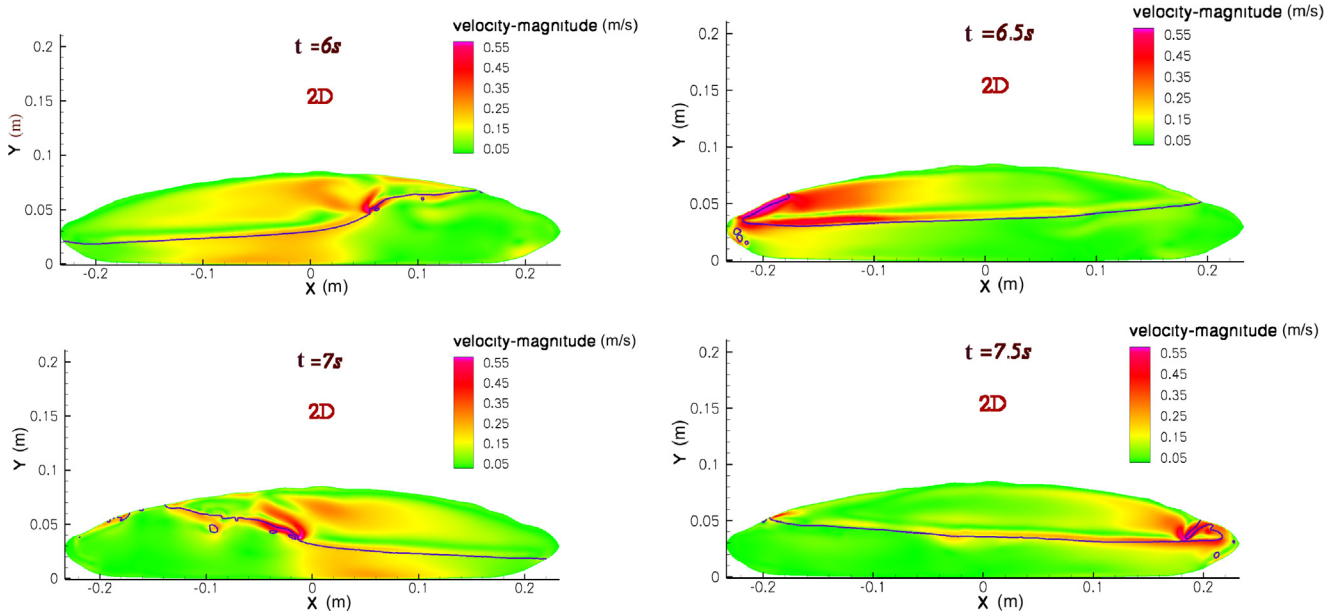

Fig. 6. 2D simulation of the velocity distribution for speed 30 rpm and angle 7° in 5 L volume, where the dark blue lines represent the gas-liquid interface, at different times in the 4th cycle.

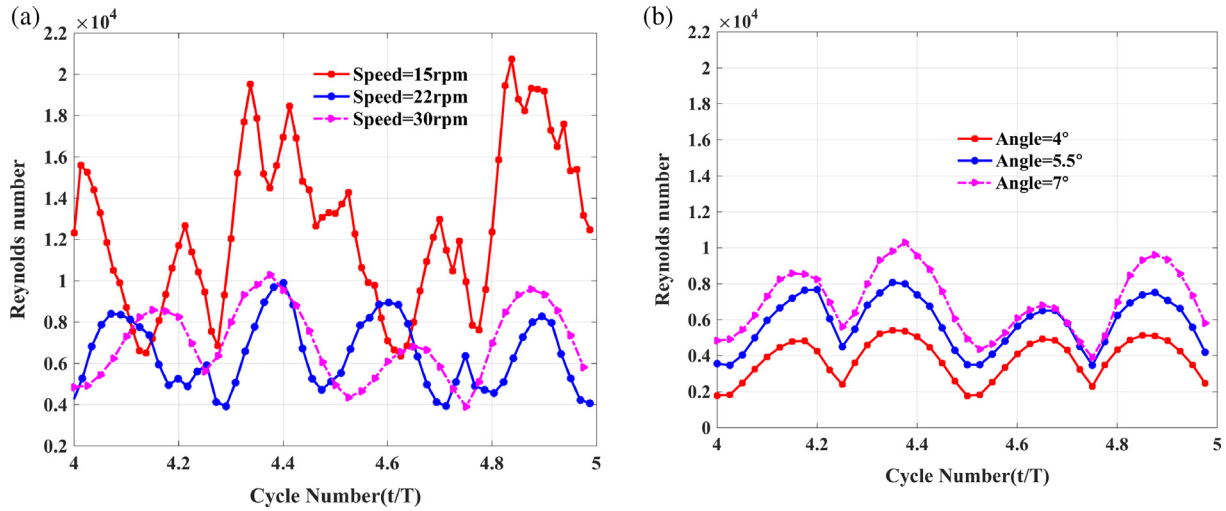

Fig. 7. Reynolds number (calculated as $\frac{uL}{v}$) during the 5th cycle (a) for speeds of 15, 22 or 30 rpm and angle 7°; (b) for angles 4°, 5.5° and 7° at speed 30 rpm by 2D simulation in 5 L volume.

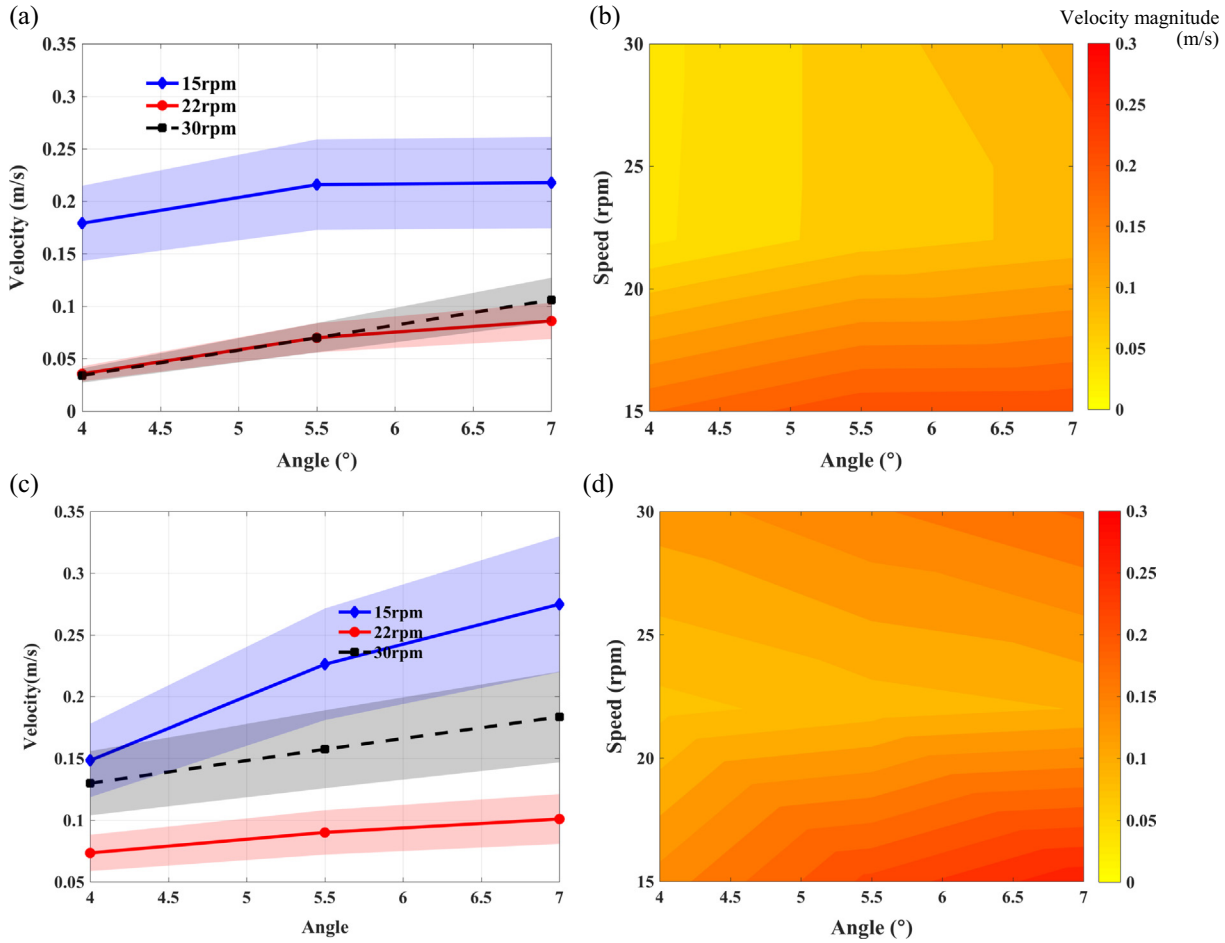

Fig. 8. 2D simulation of the average velocity for different operating conditions of cellbag speeds (15, 22 and 30 rpm) and angles (4°, 5.5°, 7°) in 5 L volume (a) and (b); and in 4 L volume (c) and (d). Shadows indicate the potential error of 20% generated in 2D simulation compared to 3D simulation.

complex small-structure and chaotic fluid conditions. The continuous high Reynolds number indicates that a chaotic fluid motion occurres at all times in a laminar flow and that efficient mixing can be achieved.

The average velocity simulated for different operating conditions at time 5 T is shown in Fig. 8. The rocking speed is the dominant effect deciding the velocity magnitude inside the cellbag as observed from Fig. 8a and b for 5 L liquid volume. Surprisingly, the lowest speed of 15 rpm generates the highest average fluid velocity and the higher speeds, 22 rpm and 30 rpm, result in lower and similar velocity in this volume. Increasing the angle leads to an enhancement of the velocity at constant speed. Notice that the average velocities obtained at 15 rpm differ from the ones at the other speeds by a value larger than 20% as indicated by the shadow zones drawn 20% away from the simulated values. Therefore the trends observed with these 2D simulations will be conserved for a 3D simulation in 5 L volume.

To support the present observations, a similar 2D simulation exercise is given in Fig. 8c–d for a volume of 4 L. In a previous report (Clincke et al., 2013b), we have studied the effect of different filling volumes on the formation of bubbles in the liquid phase in preparation for high cell density culture and showed that filing volumes of 4 L and 5 L (which is the full capacity of this equipment according to the manufacturer) result in different outcomes. Fig. 8c–d shows that for a volume of 4 L, the average velocity is also the highest at 15 rpm for all angles compared to 22 and 30 rpm. Notice however that for the smallest angle of 4° the difference is not significant taking into account the potential error of 20% of 2D compared to 3D simulation. For all the cases, the average velocity is higher in 4 L volume compared to 5 L. This is expected since the ratio of the liquid volume to the total volume is larger in the case of 4 L vs. 5 L. In other words, the liquid has a larger volume for its displacement in the cellbag and is submitted to a larger volumetric power input in the case of the smallest volume.

To quantify the mixing, the vorticity, defined as the curl (or rotational) of the flow velocity vector $\vec{\mathbf{u}}$, is investigated. By definition, the vorticity $\vec{\boldsymbol{\omega}}$ can be expressed as (Kundu and Cohen, 1990):

$$\vec{\boldsymbol{\omega}} = \nabla \times \vec{\mathbf{u}} \tag{12}$$

The components of the vorticity for the flow velocity vector $\vec{\mathbf{u}}(u_x, u_y, u_z)$ in Cartesian coordinates are:

$$\boldsymbol{\omega}_1 = \frac{\partial u_z}{\partial y} - \frac{\partial u_y}{\partial z} \quad \boldsymbol{\omega}_2 = \frac{\partial u_x}{\partial z} - \frac{\partial u_z}{\partial x} \quad \boldsymbol{\omega}_3 = \frac{\partial u_y}{\partial x} - \frac{\partial u_x}{\partial y} \tag{13}$$

For a two-dimensional flow, the vorticity is different from zero only in the out-of-plane direction

$$\boldsymbol{\omega} = \frac{\partial u_y}{\partial x} - \frac{\partial u_x}{\partial y} \tag{14}$$

In this last case, the vorticity is always perpendicular to the *XY*-plane of the flow, and is the line integral around a closed curve of the velocity vector $\vec{\mathbf{u}}$.

The vorticity magnitudes in the liquid phase for 15 and 30 rpm speeds with angle 7° are represented in Fig. 9. The highest vorticity occurs along the interface of the gas and liquid phases and along

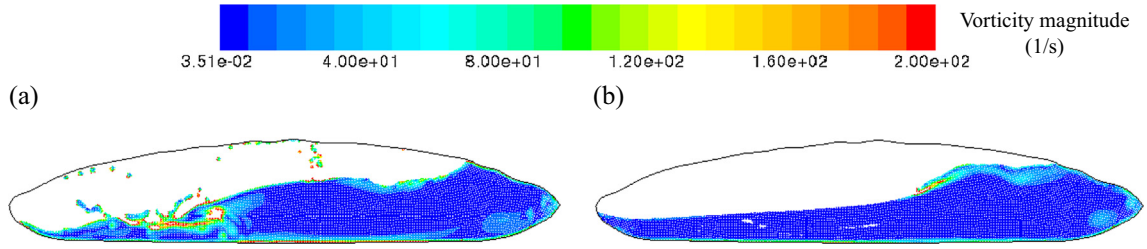

Fig. 9. Vorticity magnitude in the liquid phase for angle 7° and (a) speed 15 rpm (b) speed 30 rpm by 2D simulation in 5 L volume.

the wall, indicating that, in these regions, the largest rotational flow takes place. Comparing the two different rocking speeds, it is observed that the flow generated by a speed of 15 rpm has higher vorticity values and larger gradients in the flow. The mixing level for this speed is thus higher than for 30 rpm speed.

The average vorticity magnitudes, represented in Fig. 10, are calculated for different operating conditions. At constant speed, increasing the angle causes a larger vorticity, and consequently enhances the mixing. Similar to the trends observed for the velocity, the maximal vorticity occurs at 15 rpm speed with an angle of 7° while further increasing the speed to 22 rpm and 30 rpm decreases the vorticity and thus the mixing. As discussed above, this is counter-intuitive.

What is mechanism behind this phenomenon? Why can the lowest speed generate the highest velocity? Here the phenomenon of resonance has to be considered. Resonance happens when an object is excited at a frequency close to its natural frequency. Noting that a liquid tank of constant depth is 'homogeneous' with respect to the wave speed, the n^{th} resonance frequency f in a rectangular tank can be approximated as follows (Romero et al., 2005):

$$f = \sqrt{\frac{ng}{4\pi L}\tanh\left(\frac{\pi hn}{L}\right)} \tag{15}$$

where L is the length of the tank and h is the height of the liquid phase in the tank.

In an elliptical tank, the equivalent fluid depth h_{eq} is determined as a function of the liquid cross-sectional area and the length L as follows:

$$h_{eq} = \frac{A_{area}}{L} \tag{16}$$

In our case, A_{area} is the elliptical surface area of a longitudinal section of the cellbag, which can be calculated as $A_{area} = \pi ab$, where a is the major radius and b is the minor radius. For the present case of half-filled 10 L cellbag, the bag dimension is 0.46 m by 0.0854 m with a liquid height of 0.04 m, and the 1st excitation frequency, i.e. first resonance, occurs at 0.6 Hz, calculated by Eqs. (15) and (16). Romero et al. (2005) observed that this approach introduced a difference with the experimental results of about 5–10%, depending on the filling level. They measured the natural frequency experimentally and showed that it increased from about 1.2 Hz up to about 1.8 Hz as the filling fraction increased from 1/8 to 7/8, for the elliptical tank (of dimension 0.302 by 0.22 m) and was 1.4 Hz for a half-filled tank. In the present case, the different rocking frequencies are 1.5 Hz, 2.3 Hz and 3.14 Hz, (corresponding to 15 rpm, 22 rpm and 30 rpm rocking speed, respectively). Among these, the rocking speed of 15 rpm with a frequency of 1.5 Hz, is the closest to the natural frequency of 0.6 Hz according to the theoretical approximation of a half-filled perfect ellipse or 0.55 Hz in the case of 4 L volume. From these calculations and the particular behavior observed at 15 rpm speed, it is concluded that at this speed, a phenomenon of resonance occurs and thus the highest velocity amplitudes are created.

3.2.2. Shear stress

Efficient mixing is indispensable for bioprocesses to avoid gradients of substrates, by-products, pH or dissolved oxygen concentration. In the previous section, the mixing has been improved by more violent flows, however this introduces high stress from chaotic flow structures. Mammalian cells are sensitive to shear or mechanical force, and many studies have shown that high levels of shear affect the viability and growth of cells (Garcia-Briones

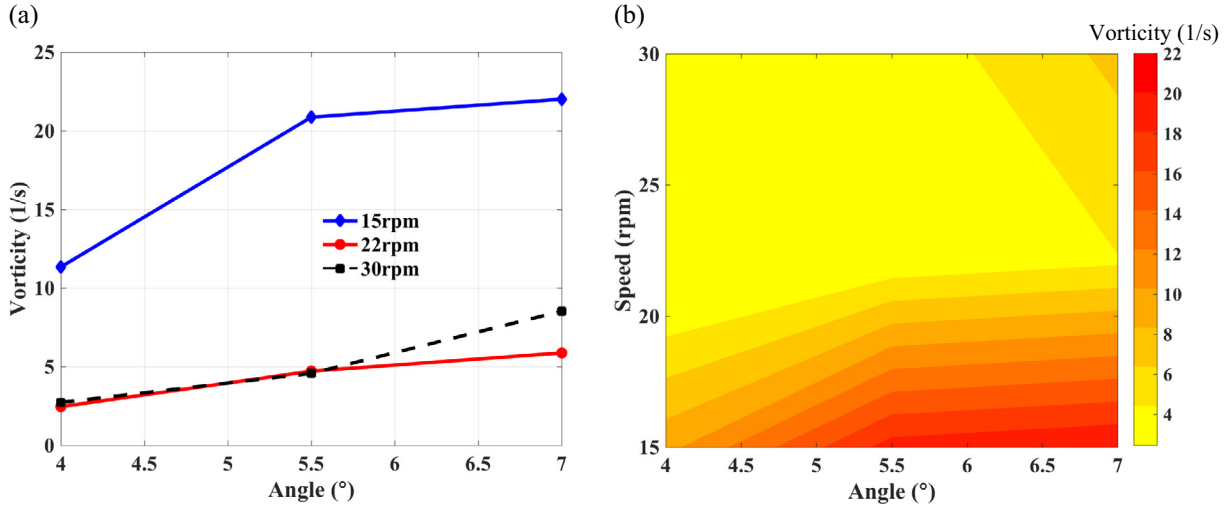

Fig. 10. Average vorticity for different operating conditions at speeds 15, 22 and 30 rpm and angles 4°, 5.5°, 7° by 2D simulation in 5 L volume.

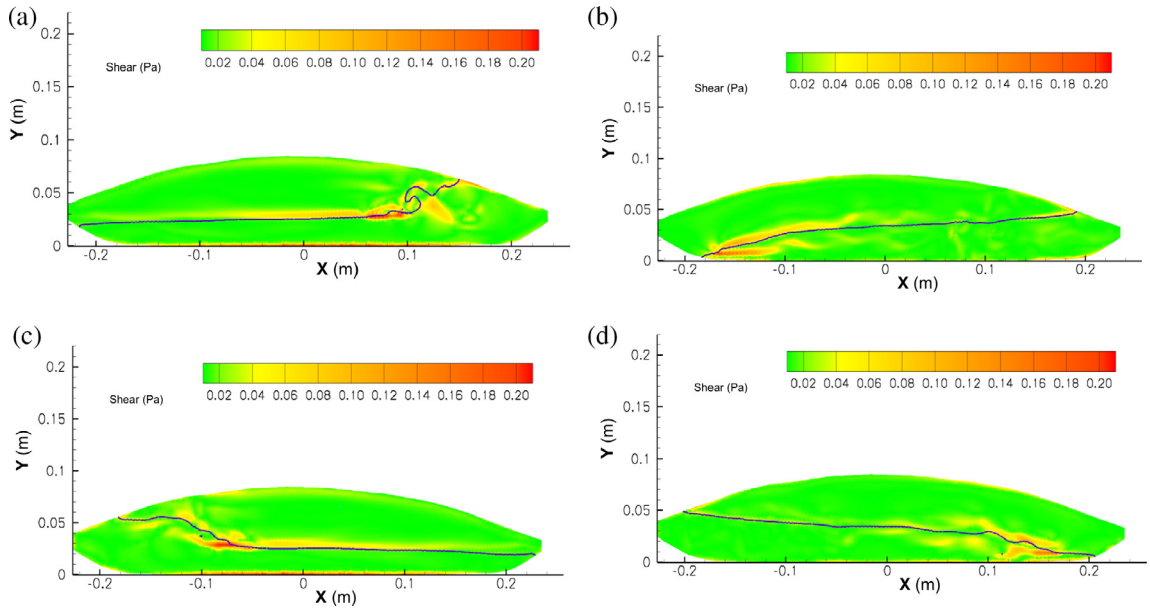

Fig. 11. Shear stress contours for speed of 30 rpm and angle 7° (the dark blue lines represent the air-water interface) at (a) t = 6 s, (b) t = 6.5 s, at (c) t = 7 s, (d) t = 7.5 s by 3D simulations in 5 L volume, with water viscosity constant and equal to 1.002×10^{-3} Pa s.

and Chalmers, 1994, Mollet et al., 2007). Shear stress should therefore be carefully considered for the choice of the operation conditions to obtain sufficient homogenization without harming the cells.

In the present simulations, the cells are considered as small particles and therefore passive tracers following the fluid flow. The velocity of a cell is the fluid velocity at a given point and can be expressed as $u_c = \mathbf{u}_{ij}$, where $\mathbf{u}_{ij}$ is the velocity of fluid at the node. The stress tensor has nine components, each of which depends on position and time.

$$\begin{bmatrix} \tau_{xx} & \tau_{xy} & \tau_{xz} \\ \tau_{yx} & \tau_{yy} & \tau_{yz} \\ \tau_{zx} & \tau_{zy} & \tau_{zz} \end{bmatrix}$$

where τ_{xx}, τ_{yy} and τ_{zz} are the three normal stress components.

The Newtonian model of fluid response is based on three assumptions:

(a) The shear stress is proportional to the rate of shear strain in a fluid particle;
(b) The shear stress is zero when the rate of shear strain is zero;
(c) The relation of stress to rate of shear strain is isotropic, i.e. there is no preferred orientation in the fluid.

In Newtonian fluids, the shear stress tensor τ_{ij} can be written as

$$\tau_{ij} = \mu\left(\frac{\delta v_i}{\delta x_i} + \frac{\delta v_j}{\delta x_j}\right) \tag{17}$$

The shear stress acting on a cell in the *XY*-plane is now considered

$$\tau_{xy} = \mu\left(\frac{\delta v_x^c}{\delta x} + \frac{\delta v_y^c}{\delta y}\right) \tag{18}$$

where μ is the liquid viscosity (which is the kinematic viscosity v multiplied by the fluid density ρ or $\mu = v\rho$) and v_x^c and v_y^c are the two components of the liquid velocity at the location of a cell.

In the case of laminar flow of Newtonian fluids, the shear stress is proportional to the fluid strain rate. The shear stress is calculated here from the rate of shear strain from the 3D simulations. As shown in Fig. 11, high stress regions occur along the gas-liquid interface with sharp velocity gradients due to the large velocity difference, and to a lower extent along the bag wall.

To study the effect of the speed and the angle on the shear stress, 2D simulations are performed in different operating conditions and the maximal shear stress in the cellbag, shown in Fig. 12, is computed. It is found that increasing the rocking angle enhances the shear stress at constant speed. This increasing trend is not systematically observed with the speed, as the lower speed of 15 rpm is associated with an increased maximal shear stress as seen in Fig. 12(b), (d) and (f). At higher speeds of 22 and 30 rpm, the maximal shear stress is comparable and smaller than that at 15 rpm speed for a given rocking angle.

In the normal operating conditions of 15–30 rpm speed and 4–7° angle, the Wave bioreactor agitation introduces a shear stress in the range of 0.005–0.06 Pa. This range is much lower than the shear stress over 1 Pa observed in a 1.4 L stirred tank bioreactor using marine impellers by Joshi et al. (1996). The critical damage shear stress for cells in suspension as single cells can be high. The death of suspended hybridoma and CHO cells occur when the cells are exposed to an energy dissipation rate of 1–5×10^4 kW/m^3 from tubing walls (Ma et al., 2002). This corresponds to shear stress values of 100–400 Pa, and is significantly higher than the values encountered in the present study.

Gregoriades et al. (2000) has observed that CHO cells attached to microcarriers are significantly more sensitive to energy dissipation rates than CHO cells in suspension. The energy dissipation rate leading to cell damage is around 1 kW/m^3, which is four orders of magnitude lower than for suspension cells.

The shear stress can also have non-lethal influence on cells cultures. The effect of shear stresses between 0.05 and 0.8 Pa on anchorage-dependent CHO cells producing human growth hormone (hGH) has been investigated by Keane et al. (2003), showing no morphological change on the cells. However the cells subjected to 0.10 Pa shear stress cease to produce hGH in absence of shear protectant pluronic or serum while this production is recovered in presence of one of these protectants. At a higher shear stress of 0.80 Pa, in presence of pluronic, the hGH cell specific productivity decreases to 49% compared to the absence of shear and the glucose uptake increases, witnessing an altered metabolism. Motobu

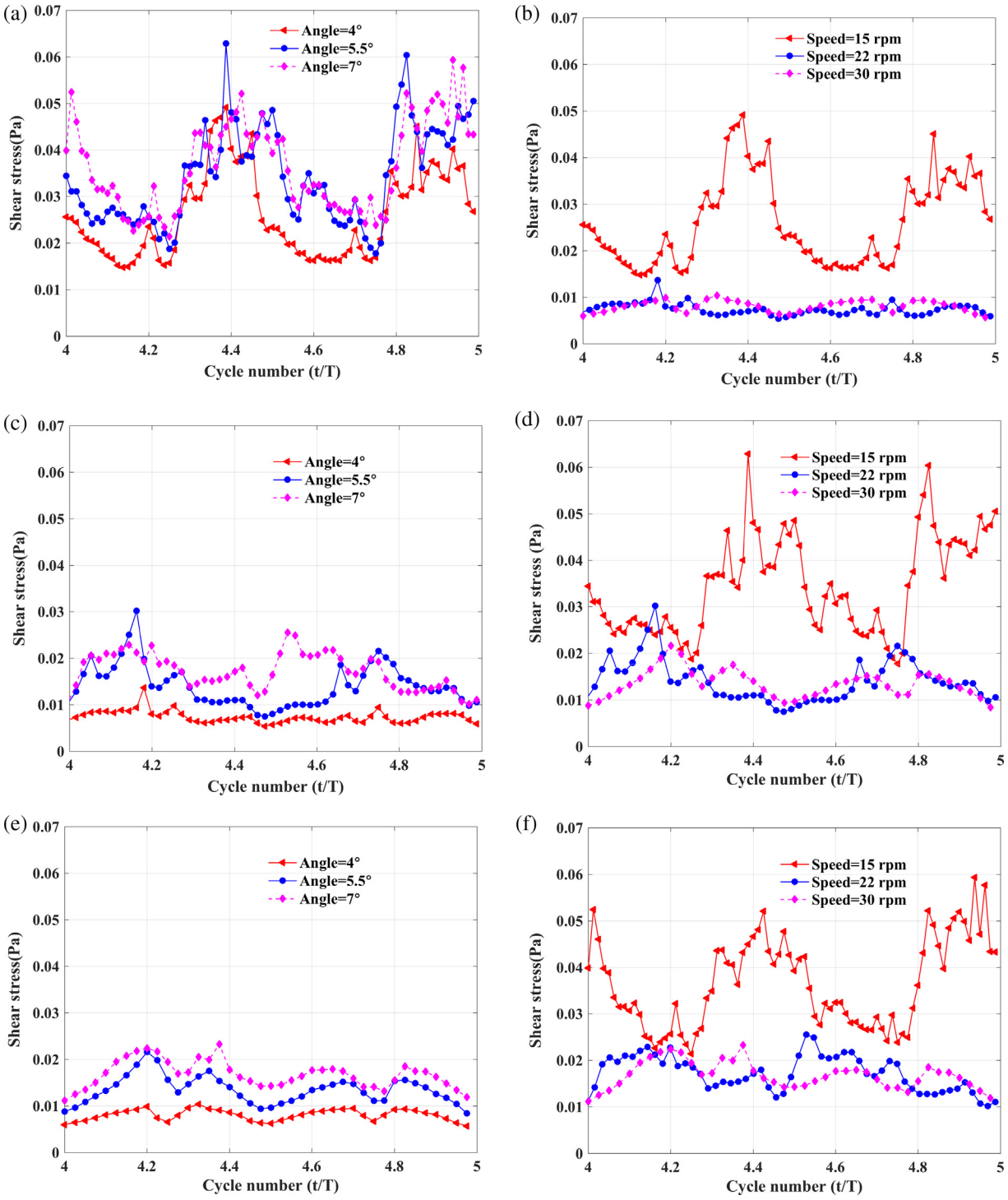

Fig. 12. 2D simulations of the maximum shear stress at speed of (a) 15 rpm, (c) 22 rpm, (e) 30 rpm and at angle (b) 4°, (d) 5.5°, (f) 7° during the 5th cycle in 5 L volume.

(Motobu et al., 1998) has reported as well that the shear stress can cause cell growth arrest in G0/G1 phase for more than 60% of CHO cells, which grow on the bottom of a flow chamber, after exposure to shear stress of 0.02 or 0.082 Pa for 24 h.

Finally, in some cases, an optimal shear stress is desirable for the formation of aggregates or embryoid bodies of stem cells or primary cells in a cell specific manner as reviewed by King and Miller (2007). They mention the examples of the mouse embryonic stem cells forming cell aggregates under an optimal shear stress of 0.61 Pa and undesired excessive clumping under a shear stress of 0.45 Pa (Cormier et al., 2006) while the optimal shear stress for the formation of aggregates in mammary epithelial stem cell culture is 0.21 Pa (Youn et al., 2005). In either cases, the shear stress range of the Wave bioreactor as reported here are too low, so that it would be recommended to form the cell aggregates in another system generating higher shear stress before continuing the culture in a Wave bioreactor for these type of cultures.

The present study indicates that at speed 15–30 rpm and angles 4–7°, the range of shear stress is potentially damageable for cell adherent on microcarriers while it is not for single cells in

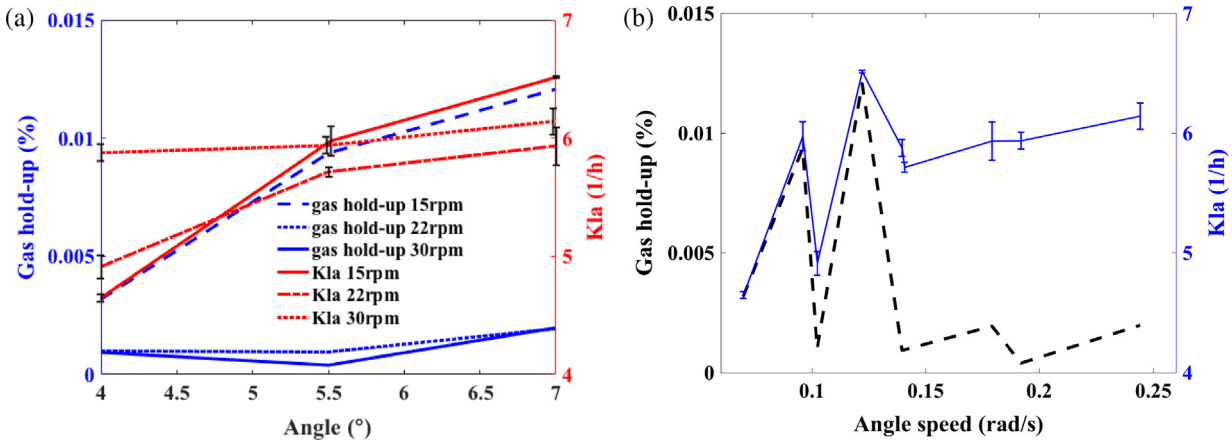

Fig. 13. (a) 2D simulation of the gas hold-up and K_La measurements as function of the rocking angle at speeds 15, 22 and 30 rpm (b) Gas hold-up and K_La as function of the angular velocity calculated by Eq. (5) for all the conditions of speeds and rocking angles in 5 L volume – Error bars indicate the standard deviation of triplicates.

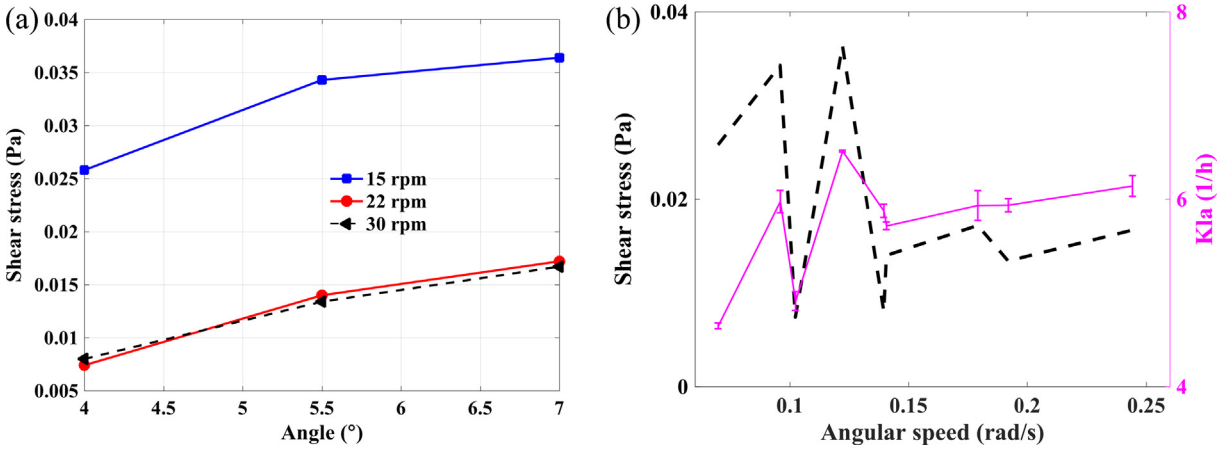

Fig. 14. (a) 2D simulation of the mean shear stress as function of the rocking angle at speeds 15, 22 and 30 rpm; (b) Shear stress and K_La as function of the angular velocity calculated by Eq. (5) for all the conditions of speeds and rocking angles in 5 L volume – Error bars indicate the standard deviation of triplicates.

suspension. This is even more critical at a speed of 15 rpm, where the shear stress is higher and can be more damageable.

3.2.3. Oxygen transfer

In this section, the oxygen transfer is simulated as well as measured in the cellbag to evaluate the potential impact of the operating conditions on the culture. Fig. 13 shows the oxygen transfer rate coefficient K_La obtained by measurements and the gas holdup, which is the ratio of the gas phase volume in the liquid phase to the total volume of the liquid phase, obtained by 2D simulations.

It is observed that both the K_La and the gas holdup increase with the angle for a given rocking speed. The maximal values of the shear stress and the K_La occur both at 15 rpm speed and the largest angle, i.e. 7°. However, at angle 5.5°, the highest K_La are observed for 15 and 30 rpm speeds, and at angle 4° the K_La increases with the speed. In other words, at angles $\leq$5.5°, the trends of the gas holdup and the K_La do not coincide. This can be due to some factors occurring in the real system but omitted in the simulation; for instance, the VOF model cannot take into account the gas transfer of the bubbles entering the liquid phase, which is occurring, in particular at higher agitation speed (Clincke et al., 2013b).

The angular velocity (Eq. (5)) includes the effects of the speed and the velocity of an element in an oscillating system. The values of the K_La and the gas hold-up are represented for the different studied conditions as function of the angular speed in Fig. 13b. It can be seen that the trends of the gas hold-up and the K_La as function of the angular speed are comparable; the highest gas hold-up leading to the largest oxygen transfer, coincides with the highest measured K_La. In addition, these results confirm also the reliability of the numerical models and simulations of the present study.

More violent flows can improve the fluid mixing, but this can also introduce high stress from chaotic flow structures. The shear stress presented in Fig. 14 is largest at a speed of 15 rpm, where the highest mixing level and thus oxygen transfer are generated.

As discussed in Section 3.2.1, a resonance phenomenon causes a higher amplitude of the fluid motion at lower rocking speed. At 15 rpm speed with 5 L working volume (i.e. half-filled volume), the frequency is close to the natural frequency of the cellbag, and the highest amplitude of the fluid motion occurs, leading to chaotic flow with complex structure. At given speed but not systematically at maximal speed, increasing the rocking angle, i.e. increasing the motion amplitude, can enhance the mixing level and the shear stress.

4. Conclusions

In this paper, we have studied the fluid dynamics in the cellbag of a Wave bioreactor by 3D and 2D numerical simulations. Several important factors for bioreactor cell cultivation, i.e. the mixing, the

shear stress and the oxygen transfer, are investigated by numerical simulations. It is found that 2D simulation, which requires significantly lower computational costs, can be used to capture the tendencies in time and phase simulated in 3D, although the simulation quality is lower. Therefore, these 2D simulations should be used for a qualitative interpretation of the liquid motion rather than quantitative.

Mixing is important in bioprocesses. It can be improved by creating a chaotic fluid flow. This means either that the flow regime is turbulent or involving complex fluid structures. Turbulent flows are chaotic in nature, but chaotic flows are not always turbulent. In laminar flows, chaotic trajectories and mixing can occur although the flow is non-turbulent. In this case, the fluid surfaces are exponentially stretched and folded, which is termed 'chaotic mixing'.

These complex fluid structure introduced by chaotic flow can lead to shear stress. Although the shear stress level is lower in a Wave bioreactor compared to stirred tank bioreactor (Joshi et al., 1996), the fluid shear stress can have a profound influence on the cells, ranging from altered metabolism to cell lysis (Croughan et al., 1987, Frangos et al., 1988, Ziegelstein et al., 1992). Referring to the shear stress levels reported in Keane et al. (2003) and in Motobu et al. (1998), in the operating conditions presently investigated (speeds 15, 22 or 30 rpm, angles 4°, 5.5° and 7°, volumes 5 L or 4 L), the encountered shear stress can lead to decreased productivity or cell growth arrest in the case of CHO cells adherent on microcarriers but not for single cells in suspension. Harsher shear stress conditions are obtained for the speed of 15 rpm due to the phenomenon of resonance and should thus be avoided for microcarrier culture in this Wave bioreactor size.

In the present operating setting, the range of shear stress necessary for the formation of aggregates or spheroids is too low according to our simulations. Therefore it seems suitable to use another system than the Wave bioreactor generating a higher shear stress for the aggregate formation and then to use this type of bioreactor for their culture.

Our results point out that a resonance phenomenon can take place in a Wave bioreactor and have a predominant effect on the fluid motion. It is shown here that the natural frequency of the bioreactor is an important factor in the dynamics, the mixing and the shear stress of the fluid in this type of reactor. It can provoke non-intuitive behavior such as high fluid motion at lower rocking speed. This could explain a phenomenon that experienced operators have observed when they tune the rocking parameters of a Wave bioreactor. The rocking and angle tuning is done manually nowadays. The approach presented here can help the selection of the operating settings generating favorable hydrodynamic conditions of oxygen transfer while minimizing the shear damage. For the cellbag sizes other than10 L studied here, it can be recommended to calculate an approximation of the natural frequency by Eqs. (15) and (16) for the tuning of the rocking speed in order to either seek to work close to this frequency if increased shear stress is favorable for the process or to avoid it in the contrary. The present study paves the way towards a systematic method to select these parameters as function of the desired mixing and shear tolerance of the cells. Finally, it can be mentioned as well that the phenomenon of resonance can have an impact on the Wave bioreactor power input and brings important information for the requirement in terms of the cellbag mechanical resistance or for the bag design.

Acknowledgements

This research was supported by the Chinese Scholarship Council and by the Competence Centre for Advanced BioProduction by Continuous Processing, AdBIOPRO, sponsored by the Sweden's Innovation Agency VINNOVA, diaries nr. 2016-05181. Many thanks to Swedish Orphan Biovitrum for providing the Wave bioreactor system and to Prof. Alper A. Öncül and Dominique Thévenin for generously providing their data.

References

Chalmers, J.J., 2015. Mixing, aeration and cell damage, 30+years later: what we learned, how it affected the cell culture industry and what we would like to know more about. Curr. Opin. Chem. Eng. 10, 94–102.
Chen, A.K., Reuveny, S., Oh, S.K., 2013. Application of human mesenchymal and pluripotent stem cell microcarrier cultures in cellular therapy: achievements and future direction. Biotechnol. Adv. 31, 1032–1046.
Clincke, M.F., Molleryd, C., Samani, P.K., Lindskog, E., Faldt, E., Walsh, K., Chotteau, V., 2013a. Very high density of Chinese hamster ovary cells in perfusion by alternating tangential flow or tangential flow filtration in WAVE bioreactor. Part II: Applications for antibody production and cryopreservation. Biotechnol. Prog. 29 (3), 768–777.
Clincke, M.F., Molleryd, C., Zhang, Y., Lindskog, E., Walsh, K., Chotteau, V., 2013b. Very high density of CHO cells in perfusion by ATF or TFF in WAVE bioreactor. Part I. Effect of the cell density on the process. Biotechnol. Prog. 29 (3), 754–767.
Cormier, J.T., Nieden, N.I., Rancourt, D.E., Kallos, M.S., 2006. Expansion of undifferentiated murine embryonic stem cells as aggregates in suspension culture bioreactors. Tissue Eng. 12, 3233–3245.
Croughan, M.S., Hamel, J.F., Wang, D.I.C., 1987. Hydrodynamic effects on animal-cells grown in microcarrier cultures. Biotechnol. Bioeng. 29 (1), 130–141.
dos Santos, F.F., Andrade, P.Z., da Silva, C.L., Cabral, J.M.S., 2013. Bioreactor design for clinical-grade expansion of stem cells. Biotechnol. J. 8 (6), 644–654.
Eibl, R., Werner, S., Eibl, D., 2009. Bag bioreactor based on wave-induced motion: characteristics and applications. Adv. Biochem. Eng. Biotechnol. 115, 55–87.
Frangos, J.A., Mcintire, L.V., Eskin, S.G., 1988. Shear-stress induced stimulation of mammalian-cell metabolism. Biotechnol. Bioeng. 32 (8), 1053–1060.
Garcia-Briones, M.A., Chalmers, J.J., 1994. Flow parameters associated with hydrodynamic cell injury. Biotechnol. Bioeng. 44 (9), 1089–1098.
Genzel, Y., Olmer, R.M., Schäfer, B., Reichl, U., 2006. Wave microcarrier cultivation of MDCK cells for influenza virus production in serum containing and serum-free media. Vaccine 24 (35–36), 6074–6087.
Gregoriades, N., Clay, J., Ma, N., Koelling, K., Chalmers, J.J., 2000. Cell damage of microcarrier cultures as a function of local energy dissipation created by a rapid extensional flow. Biotechnol. Bioeng. 69 (2), 171–182.
Hundt, B., Best, C., Schlawin, N., Kassner, H., Genzel, Y., Reichl, U., 2007. Establishment of a mink enteritis vaccine production process in stirred-tank reactor and Wave((R)) Bioreactor microcarrier culture in 1–10L scale. Vaccine 25 (20), 3987–3995.
Joshi, J.B., Elias, C.B., Patole, M.S., 1996. Role of hydrodynamic shear in the cultivation of animal, plant and microbial cells. Chem. Eng. J. 62 (2), 121–141.
Keane, J.T., Ryan, D., Gray, P.P., 2003. Effect of shear stress on expression of a recombinant protein by Chinese hamster ovary cells. Biotechnol. Bioeng. 81 (2), 211–220.
King, J.A., Miller, W.M., 2007. Bioreactor development for stem cell expansion and controlled differentiation. Curr. Opin. Chem. Biol. 11, 394–398.
Kundu, P., Cohen, L., 1990. Fluid Mechanics. Elsevier Science (USA).
Kurzweg, U.H., Lindgren, E.R., Lothrop, B., 1989. Onset of turbulence in oscillating flow at low Womersley number. Phys. Fluids A 1 (12), 1972–1975.
Liu, N., Zang, R., Yang, S.T., Li, Y., 2014. Stem cell engineering in bioreactors for large-scale bioprocessing. Eng. Life Sci. 14 (1), 4–15.
Lohr, V., Rath, A., Genzel, Y., Jordan, I., Sandig, V., Reichl, U., 2009. New avian suspension cell lines provide production of influenza virus and MVA in serum-free media: studies on growth, metabolism and virus propagation. Vaccine 27 (36), 4975–4982.
Ma, N.N., Koelling, K.W., Chalmers, J.J., 2002. Fabrication and use of a transient contractional flow device to quantify the sensitivity of mammalian and insect cells to hydrodynamic forces. Biotechnol. Bioeng. 80 (4), 428–437.
Mollet, M., Godoy-Silva, R., Berdugo, C., Chalmers, J.J., 2007. Acute hydrodynamic forces and apoptosis: a complex question. Biotechnol. Bioeng. 98 (4), 772–788.
Morrow, K., 2006. Disposable bioreactors gaining favor. Genet. Eng. News 26 (12), 42-+.
Motobu, M., Wang, P.C., Matsumura, M., 1998. Effect of shear stress on recombinant Chinese hamster ovary cells. J. Ferment. Bioeng. 85 (2), 190–195.
Noh, W.F., Woodward, P., 1976. SLIC (Simple Line Interface Calculation). Springer Berlin Heidelberg, Berlin, Heidelberg.
Okonkowski, J., Balasubramanian, U., Seamans, C., Fries, S., Zhang, J., Salmon, P., Robinson, D., Chartrain, M., 2007. Cholesterol delivery to NSO cells: challenges and solutions in disposable linear low-density polyethylene-based bioreactors. J. Biosci. Bioeng. 103 (1), 50–59.
Öncül, A.A., Kalmbach, A., Genzel, Y., Reichl, U., Thevenin, D., 2010. Characterization of flow conditions in 2 L and 20 L wave bioreactors (R) using computational fluid dynamics. Biotechnol. Prog. 26 (1), 101–110.
Romero, J.A., Hildebrand, R., Martinez, M., Ramirez, O., Fortanell, J.M., 2005. Natural sloshing frequencies of liquid cargo in road tankers. Int. J. Heavy Veh. Syst. 12 (2), 121–138.
Schnitzler, A.C., Verma, A., Kehoe, D.E., Jing, D.H., Murrell, J.R., Der, K.A., Aysola, M., Rapiejko, P.J., Punreddy, S., Rook, M.S., 2016. Bioprocessing of human

mesenchymal stem/stromal cells for therapeutic use: current technologies and challenges. Biochem. Eng. J. 108, 3–13.
Sharma, C., Malhotra, D., Rathore, A.S., 2011. Review of Computational fluid dynamics applications in biotechnology processes. Biotechnol. Prog. 27 (6), 1497–1510.
Singh, H., Hutmacher, D.W., 2008. Bioreactor Studies and Computational Fluid Dynamics.
Singh, V., 1999. Disposable bioreactor for cell culture using wave-induced agitation. Cytotechnology 30 (1–3), 149–158.
Williams, K.A., Saini, S., Wick, T.M., 2002. Computational fluid dynamics modeling of steady-state momentum and mass transport in a bioreactor for cartilage tissue engineering. Biotechnol. Prog. 18 (5), 951–963.
Youn, B.S., Sen, A., Kallos, M.S., Behie, L.A., Girgis-Gabardo, A., Kurpios, N., Barcelon, M., Hassell, J.A., 2005. Large-scale expansion of mammary epithelial stem cell aggregates in suspension bioreactors. Biotechnol. Prog. 21, 984–993.
Ziegelstein, R.C., Cheng, L., Capogrossi, M.C., 1992. Flow-dependent cytosolic acidification of vascular endothelial-cells. Science 258 (5082), 656–659.